Journal of Power Sources 195 (2010) 2520–2525

Contents lists available at ScienceDirect

Journal of Power Sources

journal homepage: www.elsevier.com/locate/jpowsour

Zirconium phosphate as the proton conducting material in direct hydrocarbon polymer electrolyte membrane fuel cells operating above the boiling point of water

Amani Al-Othman[a,b], André Y. Tremblay[a], Wendy Pell[b], Sadok Letaief[b], Tara J. Burchell[c], Brant A. Peppley[d], Marten Ternan[e,*]

[a] Chemical and Biological Engineering, University of Ottawa, 161 Louis Pasteur, Ottawa, ON K1N 6N5, Canada
[b] Catalysis Centre for Research and Innovation, University of Ottawa, 161 Louis Pasteur, Ottawa, ON K1N 6N5, Canada
[c] Department of Physics, University of Ottawa, 161 Louis Pasteur, Ottawa, ON K1N 6N5, Canada
[d] Chemical Engineering, Queens University, Dupuis Hall, Kingston, ON K7L 3N6, Canada
[e] EnPross Inc., 147 Banning Road, Ottawa, ON K2L 1C5, Canada

ARTICLE INFO

Article history:
Received 5 October 2009
Received in revised form
12 November 2009
Accepted 12 November 2009
Available online 18 November 2009

Keywords:
Zirconium phosphate
Proton conductivity
Direct hydrocarbon fuel cells
Impedance spectroscopy
Hydration

ABSTRACT

Zirconium phosphate (ZrP) was investigated as a possible proton conductor material in direct hydrocarbon polymer electrolyte membrane (PEM) fuel cells that operate at greater temperatures than conventional PEM fuel cells. Amorphous zirconium phosphate was synthesized in this work by precipitation at room temperature via reaction of $ZrOCl_2$ with H_3PO_4 aqueous solutions. The conductivity of the synthesized ZrP materials were 7.04×10^{-5} S cm^{-1} for ZrP oven dried in laboratory air at 70 °C and 3.57×10^{-4} S cm^{-1} for ZrP powder dried first at 70 °C in laboratory air and then processed at 200 °C with continuous H_2O injection at an H_2O/N_2 molar ratio of 6. This work showed that by maintaining appropriate water content in the vapour phase at processing conditions, it was possible to alter the composition of zirconium phosphate to a sufficiently hydrated state, and thereby avoid the normal decrease in conductivity with increasing temperature.

1. Introduction

Work in our laboratory is being directed toward the development of direct hydrocarbon fuel cells having an electrolyte membrane containing zirconium phosphate as its proton conductor component. Hydrogen is the fuel used in most fuel cells. Methanol is the second most common fuel. The reason that hydrocarbons are normally not fed directly to the anode of a fuel cell is that fuel cell performance with hydrocarbon fuels is much worse than with hydrogen or methanol.

Increasing the fuel cell operating temperature is expected to improve the reaction kinetics and therefore improve hydrocarbon fuel cell performance. Nafion™, the polymer electrolyte membrane (PEM) used in many hydrogen fuel cells becomes dehydrated as the temperature increases and is not suitable at temperatures greater than 85 °C. In contrast, composite electrolytes composed of zirconium phosphate, Nafion™, and polytetrafluoroethylene (PTFE) have been used in hydrogen fuel cells at temperatures up to 120 °C [1]. Although functional, the performance does decrease as the temperature rises above 80 °C. The target temperature for this work is 200 °C.

For a direct propane fuel cell, the overall reaction at the anode is:

$$C_3H_8 + 6H_2O = 3CO_2 + 20H^+ + 20e^- \quad (1)$$

Therefore, for a steady-state reaction, the feedstock must contain 6 moles of water for every mole of propane. In contrast when hydrogen is the fuel there is no stoichiometric requirement to include water in the feedstock. Although the hydrogen feedstock to a hydrogen fuel cell is often humidified, the saturated water vapour pressure at the anode of hydrogen fuel cells is small compared to the stoichiometric quantity in Eq. (1).

Zirconium hydrogen phosphate $Zr(HPO_4)_2$ (abbreviated as ZrP) is a solid protonic conductor. ZrP has a layered structure that allows the intercalation of guest molecules. It has cationic exchange properties, proton conducting properties, and is a highly hydroscopic insoluble solid. The interest in this compound goes back to the 1950s since its behaviour as a cation exchanger [2–4] was discovered. The cationic exchange behaviour was explained by the layered structure and the presence of passageways that provide a

* Corresponding author. Tel.: +1 613 831 8079; fax: +1 613 831 5458.
E-mail address: ternan@sympatico.ca (M. Ternan).

0378-7753/$ – see front matter © 2009 Elsevier B.V. All rights reserved.
doi:10.1016/j.jpowsour.2009.11.052

sufficiently free volume to allow unhydrated cations to exchange [5].

Work on the conductance properties of ZrP was reported by Alberti et al. [6,7]. It was shown that the conductance of ZrP decreased with an increase in the degree of crystallinity. The fraction of the surface protons is small but their mobility is greater than these internal ones. Their combination results in a large proton conductivity. Alberti et al. [7] found that the mobility of surface ions in α-ZrP are 10^4 times higher than interlayer ions. Therefore, high proton conductivity is the result of the high proton mobility on the surface of ZrP.

There has been an increasing interest not only in the preparation of inorganic proton conductors, such as zirconium phosphate, but also in their use for the operation in sensors, water electrolysis units and electrochemical devices such as fuel cells. The conductivity of amorphous ZrP in water at 80 °C approaches 0.01 S cm^{-1} [8]. This has triggered several studies in literature to evaluate the proton conductivity of ZrP after its incorporation within non-conductive materials such as polymers [9]. Examples are composite membranes prepared by the precipitation of zirconium phosphate in situ in polytetraflouroethylene (PTFE) [10], in Nafion™ [1,10], and in the composites prepared by Park et al. [11] by mixing the PTFE emulsion and the ZrP powder followed by drying and pressing.

The object of this work is to investigate ZrP as an electrolyte material for hydrocarbon fuel cells: specifically, to (1) investigate the degree of ZrP hydration at high temperatures and (2) investigate the effect of hydration on conductivity.

2. Experimental

2.1. Preparation and characterization of zirconium phosphate powder (ZrP)

Zirconium phosphate powder (ZrP) was prepared by the reaction of aqueous solutions of zirconium oxychloride ($ZrOCl_2$) and phosphoric acid (H_3PO_4). A 100 mL (0.5 M) solution of $ZrOCl_2$ was prepared using $ZrOCl_2 \cdot 8H_2O$ purchased from Aldrich. The ZrP powder was precipitated at room temperature upon the addition of 1 M of H_3PO_4 in three stages. The precipitation reaction proceeded according to the following equation:

$$ZrOCl_2 + 2H_3PO_4 \rightarrow Zr(HPO_4)_2 + 2HCl + H_2O \quad (2)$$

The gel, formed by the reaction, was then filtered and washed five times with de-ionized water. The samples obtained were heated to different temperatures. These samples were subjected to various characterization methods.

The various ZrP samples were subjected to one of two different sets of environmental conditions. The first set of environmental conditions involved heat treatment in laboratory air for 24 h, as follows: (a) ZrP powder oven dried at 70 °C in laboratory air (i.e. at a relative humidity of 20%); (b) ZrP powder oven dried at 110 °C in laboratory air; (c) ZrP powder oven dried first at 70 °C and then at 200 °C both in laboratory air. The second set of environmental conditions was a combination of heat treatment and elevated water vapour pressure, specifically: (d) ZrP powder dried first at 70 °C in laboratory air and then processed at 200 °C in a tube furnace, for 3 h with continuous H_2O injection at an H_2O/N_2 molar ratio of 6, the stoichiometric ratio in the direct propane fuel cell reaction, as shown in Fig. 1. After the above processing, each sample was placed in a closed bag made of non-porous PTFE and sent for analysis.

2.2. Conductivity measurements (impedance spectroscopy)

The electrochemical impedance of ZrP electrolyte was measured using a common electrochemical cell that is shown in Fig. 2. 304 stainless steel was used to construct the cell electrodes. The design of the cell was taken from Wang et al. [12]. The cell was cylindrical in shape with an inside diameter of 7.08 mm. A 304 stainless steel bolt (24 threads per inch, or pitch = 1.058 mm per thread) could be screwed into one end of the ceramic cylinder. The other end of the ceramic cylinder was also threaded and was connected to a 304 stainless steel base. A typical pellet would have a diameter of 7 mm and a thickness of 0.7 mm.

The resultant ZrP samples were crushed to form a fine powder. The powder was placed in the cell and compressed until a constant torque was obtained. The resulting pellet was used for the conductivity measurements. The torque applied to the cell was measured with a torque wrench and had a value of 40 lb_F in (4.5 Nm). The load, F, used to compress the powder was calculated from the torque, T, using an empirical engineering formula, $F = 0.2DT$, where D is the nominal bolt diameter and 0.2 is the "nut" factor. The pressure, $P = F/A$, where A is the cross-sectional area of the flat end of the bolt was determined to be 300 kPa.

The four probe EIS (electrochemical impedance spectroscopy) measurements were made using a Parstat 2273 electrochemical measurement system running electrochemical Power Suite software over a frequency range of 1–100 kHz with an applied voltage of ±10 mV. For each sample tested, a value for the electrolyte resistance was derived from the impedance experiments. Nyquist plots were obtained from impedance data. A typical Nyquist plot obtained during this work was composed of a small portion of a semi-circle at high frequencies followed by a Warburg tail that approaches a straight line, at low frequencies. The data at the very highest frequencies in Fig. 3 show a short line that is almost vertical. It is one end of the semi-circle. Data obtained with less compacted ZrP material, not shown in this work, formed a complete semi-

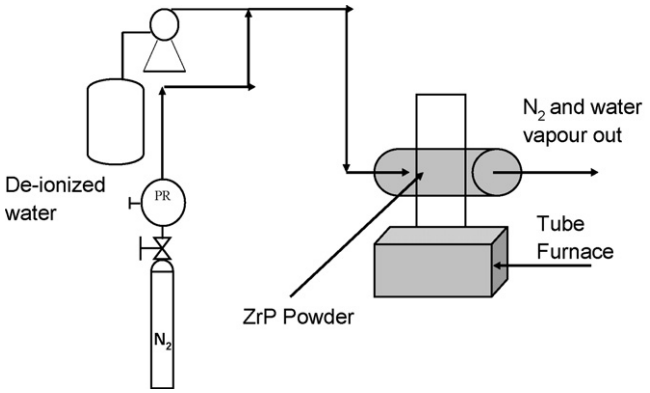

Fig. 1. H_2O partial pressure experiment equipment.

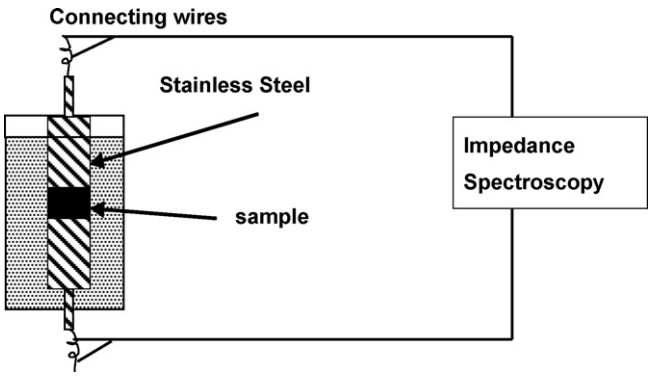

Fig. 2. Impedance spectroscopy cell.

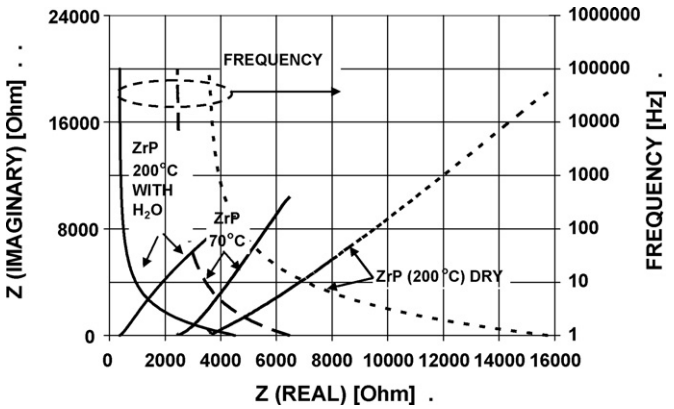

Fig. 3. Nyquist plot for ZrP samples (ZrP powder dried at 70 °C in laboratory air; ZrP powder dried at 200 °C in laboratory air; and ZrP powder dried first at 70 °C in laboratory air and then processed at 200 °C in a tube furnace with continuous H_2O injection at an H_2O/N_2 molar ratio of 6, the stoichiometric ratio in the direct propane fuel cell reaction).

circle. The straight line in the Nyquist plot can be extrapolated to its intersection with the *x*-axis to obtain a value of resistance. The conductivity (σ) in S cm^{-1} was then calculated [11] according to the equation:

$$\sigma = \frac{d}{RA} \quad (3)$$

where *d* and *A* are the thickness and the area for the sample respectively. Values of the electrolyte resistances, *R*, were obtained from Nyquist plots.

2.3. Samples characterization

The samples were analysed by XRD (X-ray diffraction) using Philips PW 1830 generator machine and TGA (Thermo Gravimetric Analysis) using a 2960 SDT analyser from TA instruments. Thermal analysis was performed under N_2 and at a heating rate of 15 and 1 °C min^{-1}.

3. Results and discussion

3.1. Conductivity measurements

The ZrP powders were analysed using electrochemical impedance spectroscopy (EIS) after being dried at various temperatures. The samples tested were (1) ZrP powder dried at 70 °C in laboratory air; (2) ZrP powder dried at 200 °C in laboratory air; (3) ZrP powder dried first at 70 °C in laboratory air and then processed at 200 °C in a tube furnace with continuous H_2O injection at an H_2O/N_2 molar ratio of 6, which is the stoichiometric ratio in the direct propane fuel cell reaction. The objective was to evaluate their conductivities. The conductivity results, measured at room temperature, are presented as Nyquist plots in Fig. 3. The frequencies are shown as a separate line in Fig. 3. In general, the conductivity plots are composed of a Warburg line at frequencies less than 100 kHz and a partial semi-circle (not visible in Fig. 3) at frequencies greater than 100 kHz [12]. The electrolyte resistance was then determined by extrapolating the Warburg portion of the plot to the *x*-axis. The intercept at the *x*-axis is the real part of the ZrP impedance.

The Nyquist plots, in Fig. 3, above provided values of ohmic resistances that were 3500 Ω after 70 °C final air drying temperature, 2400 Ω after 200 °C final air drying temperature and 375 Ω after 200 °C final processing temperature with a H_2O/N_2 molar ratio of 6. These resistance values along with the thickness and the area of the sample were used in Eq. (3) to calculate the conductivity, σ, in S cm^{-1}. The results are shown in Table 1. It can be seen that the conductivity decreased from 7.04×10^{-5} to 5.79×10^{-5} S cm^{-1} with the increase in the final drying temperature (in laboratory air) from 70 to 200 °C. This is typical behaviour. As the temperature increases, water evaporates and condensation of the hydroxyl groups in ZrP occurs. Loss of protons as a result causes the conductivity to decrease considerably [13]. The above results are also in agreement with previous conclusions that the transport of ions in ZrP is protonic via the Grothuss mechanism [14] as the conductivity decreases with the loss of protons. More importantly our experimental data in Table 1 show that by maintaining the ZrP material in an atmosphere that is predominantly water, the proton conductivity (3.57×10^{-4} S cm^{-1}) is almost an order of magnitude greater than when it is in a relatively dry atmosphere (5.79×10^{-5} S cm^{-1}).

Table 1
Experimental conductivity values as a function of processing conditions.

Processing conditions	Proton conductivity (S cm^{-1})
70 °C air drying	7.04×10^{-5}
200 °C air drying	5.79×10^{-5}
200 °C processing at an H_2O/N_2 molar ratio of 6	3.57×10^{-4}

ZrP proton conductivities have been reported in previous studies. For instance, the proton conductivities of the crystalline phase α-ZrP, $Zr(HPO_4)_2 \cdot H_2O$, were: 9.4, 3.7 and 3×10^{-5} S cm^{-1} [5,15]. These results are consistent with the conclusion that the conductivity decreases with the degree of crystallinity. Patel and Chudasama [13] and Thakkar et al. [16] have reported that amorphous ZrP pellets had protonic conductivity values of 4.2×10^{-6} to 1.9×10^{-6} S cm^{-1} over the temperature range of 30–120 °C respectively. Casciola and Bianchi [17] have also reported a value of 3.2×10^{-6} S cm^{-1} at 30 °C for ZrP conductivity. These values have been summarized in Table 2 where it can be seen that the conductivity of ZrP decreases with temperature.

As mentioned above, our experimental results showed that a conductivity of 3.57×10^{-4} S cm^{-1} was obtained with water injection. This water-injection technique was successful in maintaining a reasonable conductivity value. In comparison 1.9×10^{-6} S cm^{-1} was reported at 120 °C under dry conditions [13]. Our own relatively dry value at 200 °C, in Table 1, was 5.79×10^{-5} S cm^{-1}. The conductivity result measured in a predominantly water atmosphere results from two factors acting against each other: (1) water injection which provides the necessary hydration to ensure proton conductivity and (2) the condensation of hydroxyl groups that occur at temperatures ~180 °C and causes a loss of proton groups [18]. The experimental results in Table 1 suggest that the first factor had the most influence.

3.2. Thermogravimetric analysis

In this work, the thermal stability of amorphous ZrP was investigated by performing thermogravimetric analyses (TGA) for the

Table 2
Conductivity values reported in the literature (S cm^{-1}).

Material	Literature values of conductivity (S cm^{-1})	Reference
$Zr(HPO_4)_2 \cdot H_2O$	9.4×10^{-5}	[5]
$Zr(HPO_4)_2 \cdot H_2O$ increasing	3.7×10^{-5}	[5]
$Zr(HPO_4)_2 \cdot H_2O$ crystallinity	3×10^{-5}	[5,15]
Amorphous ZrP at 30 °C	3.2×10^{-6}	[17]
Amorphous ZrP at 30 °C	4.2×10^{-6}	[13]
Amorphous ZrP at 120 °C	1.9×10^{-6}	[13,16]

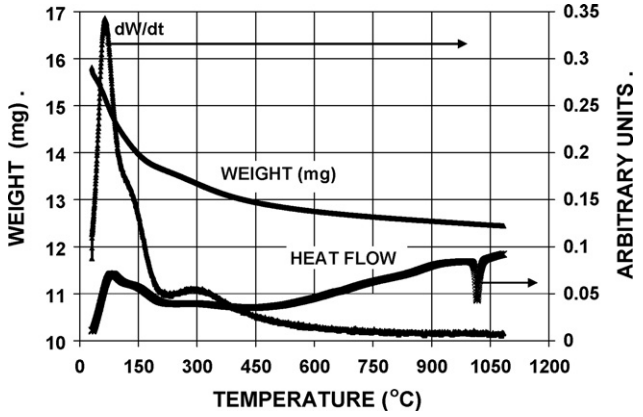

Fig. 4. TGA data for the ZrP sample that was previously dried at 70 °C and was subjected to water injection at 200 °C. [Heat flow values ($W\,g^{-1}$) were divided by −1000 to match the scale of the other two plots: (a) dW/dt ($mg\,min^{-1}$) and (b) weight (mg).]

same samples described above. The TGA analyses were performed at a heating rate of 15 °C min^{-1} in a N_2 atmosphere.

The TGA results for the sample that produced the best impedance analysis performance (200 °C–wet) are shown in Fig. 4. The TGA analysis showed a weight loss of 2.14 mg in the temperature range (25–210 °C) with a maximum in the rates of weight loss at 65 °C and an inflection point at 141 °C. The weight loss (1.15 mg) in the temperature range (210–1100 °C) had a maximum in the rate of weight loss at 304 °C.

The thermal behaviour of ZrP as ion exchangers has been the subject of several previous studies. The studies concluded that: (1) the TGA results are a function of heating rate, preparation method and properties of the starting materials and (2) there is a condensation reaction that takes place between P–OH groups and leads to a mixture of phosphate–pyrophosphate phases [19].

3.3. X-ray diffraction results

A ZrP sample was examined by X-ray diffraction (XRD) after calcination at 1100 °C for 1 h. The spectrum is shown in the lower part of Fig. 5. The spectrum was identified as the crystalline structure of zirconium pyrophosphate (ZrP_2O_7). One interesting observation in Fig. 4 is the occurrence of a sharp exothermic peak in the heat flow at 1015 °C indicating a phase change. This is explained by the

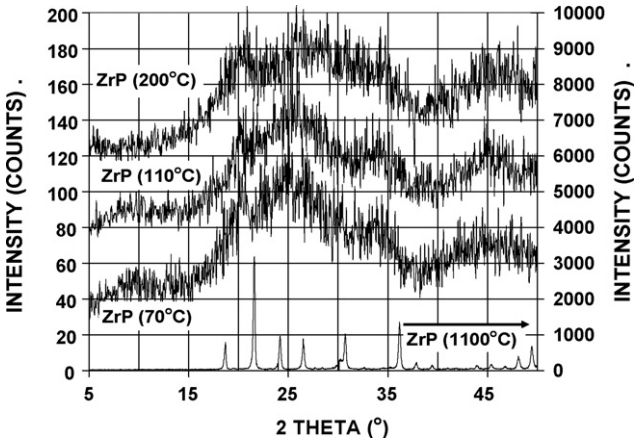

Fig. 5. XRD pattern for ZrP samples dried in laboratory air at 70, 110 and 200 °C respectively plus a ZrP sample that was calcined at 1100 °C for 1 h.

Table 3
Experimental conductivity values as a function of the material's processing conditions.

Processing conditions	A	B	C
70 °C air drying	83.34	3.72	367.98
200 °C air drying	77.09	2.39	367.97
200 °C processing at an H_2O/N_2 molar ratio of 6	77.19	4.09	594.62

transformation of layered pyrophosphate to cubic pyrophosphate that occurs at this temperature range [19–22]. Since there was no accompanying change in weight, the change in heat flow was not caused by a loss of material. These results indicate that heating to a sufficient temperature ultimately converts hydrated zirconium phosphate to zirconium pyrophosphate.

The XRD pattern for the hydrated ZrP samples that were air-dried at various temperatures are also shown in Fig. 5. Although they do not have nice crystalline patterns, like the zirconium pyrophosphate, they do have some less intensive peaks indicating that they are not completely amorphous and that they do have some structure. These patterns are characteristic of ZrP formed from the precipitation reaction of $ZrOCl_2$ and H_3PO_4 solutions at room temperature [3,13].

3.4. Analysis of the TGA data

The combination of the XRD data in Fig. 5 showing that zirconium pyrophosphate is formed above 1015 °C, and the TGA data in Fig. 4 showing that the weight at temperatures above 1015 °C is approaching a constant value, suggests a basis for analyzing the TGA data. Specifically, it suggests that all samples when heated sufficiently will approach a constant weight in the form of zirconium pyrophosphate. Therefore, the TGA weight data above 500 °C were fitted to the following empirical equation:

$$y = A + \frac{B}{\exp[(T - 500)/C]} \quad (4)$$

where T is the temperature (°C), y is the weight of the ZrP pellet, A is the weight of the ZrP sample at $T = \infty$, $B = y(T_{500}) - y(T_\infty)$, and C is an arbitrary parameter. The values of the parameters are shown in Table 3.

Fitting using Eq. (4) resulted in an excellent agreement between the calculated line and the TGA experimental data (shown as diamonds in Fig. 6). The insert in Fig. 6 shows both the diamond experimental data points and the calculated straight line. The data points are so close together in the main plot in Fig. 6 that it is impos-

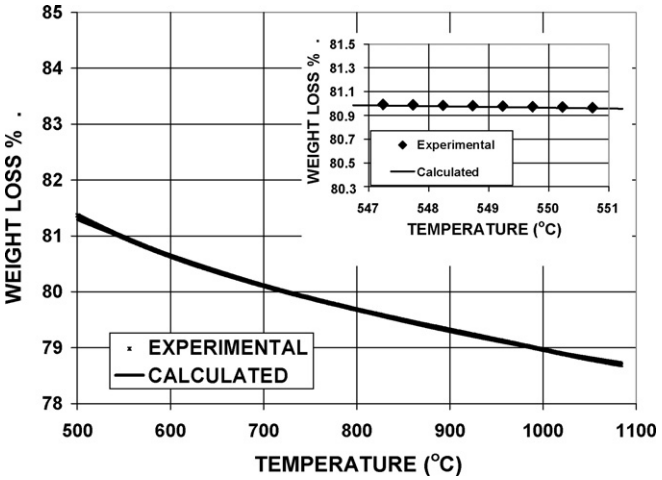

Fig. 6. The agreement between the TGA experimental data (solid diamonds) and the values calculated using Eq. (4).

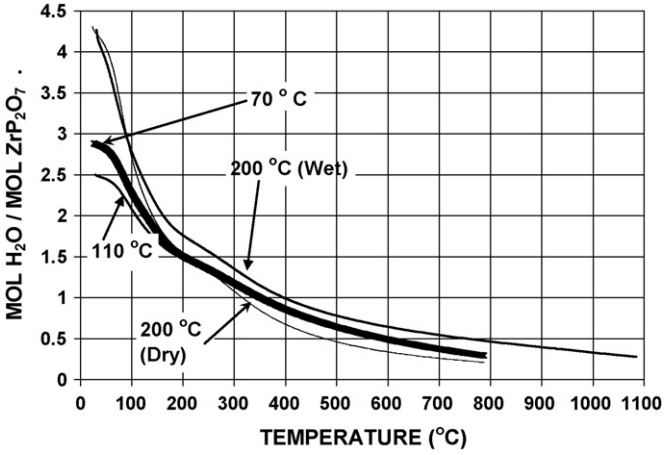

Fig. 7. TGA data fitting for ZrP samples dried at 70, 110 and 200 °C in the oven plus ZrP at 200 °C with H_2O injection (200 °C–wet).

sible to distinguish between the trajectory of diamond data points and the line calculated from Eq. (4). Eq. (4) was used to calculate the weight of zirconium pyrophosphate that would be produced from all ZrP samples when their temperatures approached $T = \infty$.

ZrP_2O_7 is formed according to the following series of reactions, each of which eliminates a water molecule:

$$ZrPO_4(H_2PO_4)\cdot xH_2O\,(x > 2) \rightarrow ZrPO_4(H_2PO_4)\cdot 2H_2O$$
$$\rightarrow Zr(HPO_4)_2\cdot H_2O \rightarrow Zr(HPO_4)_2 \rightarrow ZrP_2O_7 \quad (5)$$

When all the water of hydration that is bound to the ZrP chemical structure has been removed then only anhydrous zirconium hydrogen phosphate [$Zr(HPO_4)_2$] remains. It is subsequently converted to zirconium pyrophosphate in the final reaction.

3.5. Quantitative water content of ZrP

With the knowledge of the zirconium pyrophosphate (ZrP_2O_7) weight and by ascribing the TGA weight loss to water, the ratio (mols H_2O/mol ZrP_2O_7) at any temperature was calculated. The results are shown in Fig. 7 as moles of H_2O per mole of ZrP_2O_7.

The states of hydration in the various zirconium phosphate compounds can be identified in terms of the H_2O/ZrP_2O_7 molar ratio shown in Fig. 7. A value of "0" in Fig. 7 represents ZrP_2O_7. A value of "1" in Fig. 7 represents $Zr(HPO_4)_2$. A value of "2" in Fig. 7 represents $Zr(HPO_4)_2\cdot H_2O$. A value of "3" in Fig. 7 represents $ZrPO_4(H_2PO_4)\cdot 2H_2O$. Any value greater than 3 represents $ZrPO_4(H_2PO_4)\cdot xH_2O$ where $x > 2$. That is the formula that is used to represent the starting material, prior to drying at any temperature. Results similar to those in Fig. 7 were obtained in previous studies such as Constantino and Ginestra [19] and Patel et al. [21]. The sample dried in laboratory air at 70 °C had a value slightly less than "3" indicating that the statistically average extent of hydration was slightly less than that of γ zirconium phosphate. The sample dried in laboratory air at 110 °C had a value of approximately "2.5" indicating that its statistically average extent of hydration was between that of γ zirconium phosphate and α zirconium phosphate. Based on the above observations, it was expected that the sample dried in laboratory air at 200 °C would have a value less than "2.5". It was found to be greater than "2.5". This sample may have picked the additional moisture by being exposed to the atmosphere for an extended period of time prior to its thermogravimetric measurement. This is consistent with the results obtained by Amphlett [20] who reported that it was possible to reconvert pyrophosphates back into phosphates upon immersion in aqueous solutions at 300 °C. Finally the sample processed at a H_2O/N_2 molar ratio of 6 was expected to have a greater value than the others since it was processed in an environment with a large water content.

The water content of all the samples in Fig. 7 decreased as the temperature increased. At all temperatures, the solid sample processed at 200 °C with a H_2O/N_2 molar ratio of 6 had a greater water content than any of all the other solid samples. This observation indicates that the presence of a water rich vapour phase produced a zirconium phosphate solid that was hydrated to a greater extent than the zirconium phosphate solids that were prepared in laboratory air. The two samples dried at 200 °C, one in the presence of a water rich vapour and the other in laboratory, air provide a direct comparison showing that the water rich vapour caused the solid to be hydrated to a greater extent.

Finally the sample processed with an H_2O/N_2 molar ratio of 6 at 200 °C had both the greatest conductivity and the largest hydrated water content compared to all other samples. This is consistent with the concept that: by maintaining an appropriate water content in the vapour phase at processing conditions, it was possible to maintain the zirconium phosphate in a sufficiently hydrated state, so that the conductivity values could also be maintained.

4. Conclusions

Two conclusions can be made related to the operation of zirconium phosphate fuel cell membranes at elevated temperatures (200 °C). (1) The decrease in proton conductivity that has sometimes been attributed to a loss in water content is consistent with our measurements of conductivity and water content that are reported here in relatively dry laboratory air from 70 to 200 °C. (2) Furthermore, it was shown that an adjustment of the vapour phase water content during processing (so that the gas phase in contact with the zirconium phosphate membrane contained an H_2O/N_2 molar ratio of 6, the stoichiometric feed ratio in a direct propane fuel cell), enhanced the hydrated water content of the zirconium phosphate material compared to when it was in the presence of a relatively dry atmosphere. In addition, our experiments showed that the conductivity of this 200 °C material having the enhanced hydrate water content was even greater than that of material that had only been at 70 °C in a relatively dry atmosphere. This finding indicates that it should be possible to operate direct hydrocarbon fuel cells at elevated temperatures, without encountering degradation in the proton conductivity of the membrane and thereby take advantage of more rapid kinetics and greater current densities.

Acknowledgments

The authors gratefully acknowledge the financial support from the Canadian federal government's Natural Sciences and Engineering Research Council and from the Ontario provincial government's Ministry of Research and Innovation (Ontario Fuel Cell Research and Innovation Network).

References

[1] Y. Si, R. Jiang, J.C. Lin, H.R. Kunz, J.M. Fenton, J. Electrochem. Soc. 151 (2004) A1820.
[2] C.B. Amphelett, L.A. McDonald, M.J. Redman, J. Inorg. Nucl. Chem. 6 (1958) 220.
[3] A. Clearfield, J.A. Stynes, J. Inorg. Nucl. Chem. 26 (1964) 117.
[4] R.P. Hamlen, J. Electrochem. Soc. 109 (1962) 746.
[5] A. Clearfield, Annu. Rev. Mater. Sci. 14 (1984) 205.
[6] G. Alberti, E. Torracca, J. Inorg. Nucl. Chem. 30 (1968) 1093.
[7] G. Alberti, M. Casciola, U. Costantino, G. Levi, G. Ricciardi, J. Inorg. Nucl. Chem. 40 (1978) 533.
[8] K. Peinemann, S.P. Nunes (Eds.), Membranes for Energy Conversion, vol. 2, p. 97.

[9] O. Savadogo, J. Power Sources 127 (2004) 135.
[10] W.G. Grot, G. Rajendran, US Patent 5,919,583 (1999).
[11] Y.I. Park, K. Jae-Dong, M. Nagai, J. Mater. Sci. Lett. 19 (2000) 1735.
[12] Y.J. Wang, Y. Pan, L. Chen, Mater. Chem. Phys. 92 (2005) 354.
[13] H. Patel, U. Chudasama, J. Chem. Sci. 119 (2007) 35.
[14] A. Clearfield, Chem. Rev. 88 (1988) 125.
[15] Y.I. Park, J.D. Kim, M. Nagai, Mater. Res. Soc. Symp. Proc. 600 (2000) 305.
[16] R. Thakkar, H. Patel, U. Chudasama, Bull. Mater. Sci. 30 (2007) 205.
[17] M. Casciola, D. Bianchi, Solid State Ionics 17 (1985) 287.
[18] G. Alberti, A. Conte, E. Torracca, J. Inorg. Nucl. Chem. 28 (1966) 225.
[19] U. Constantino, A.L. Ginestra, Thermochim. Acta 58 (1982) 179.
[20] C.B. Amphlett, Inorganic Ion Exchangers, Elsevier, London, 1964, p. 107.
[21] H.K. Patel, R.S. Joshi, U. Chudasama, Indian J. Chem. 47A (2008) 348.
[22] U. Constantino, R. Vivani, V. Zima, E. Cernoskova, J. Solid State Chem. 132 (1997) 17.